Journal of Alloys and Compounds 979 (2024) 173575

Contents lists available at ScienceDirect

Journal of Alloys and Compounds

journal homepage: www.elsevier.com/locate/jalcom

Research article

Exploring the magnetic and magnetocaloric behavior of nanocrystalline melt-spun R_2Fe_{17} (R = Pr, Nd) ribbons

J.L. Garrido Álvarez [a], P. Álvarez-Alonso [a,b], C.F. Sánchez-Valdés [a,c], J.A. Blanco [a], Pedro Gorria [a,b,*], J.L. Sánchez Llamazares [a,d,*]

[a] Departamento de Física, Universidad de Oviedo, Calvo Sotelo 18, 33007 Oviedo, Spain
[b] IUTA, Universidad de Oviedo, 33203 Gijón, Spain
[c] Depto de Física y Matemáticas, División Multidisciplinaria, Ciudad Universitaria, Instituto de Ingeniería y Tecnología, Universidad Autónoma de Ciudad Juárez (UACJ), Ciudad Juárez, 32310 Chihuahua, Mexico
[d] Instituto Potosino de Investigación Científica y Tecnológica A.C., Camino a la Presa San José 2055, Col. Lomas 4ª, 78216 San Luis Potosí, Mexico

ARTICLE INFO

Keywords:
Nanostructured R_2Fe_{17} intermetallic compounds (R= Pr, Nd)
Melt-spun ribbons
Structure and magnetic properties
Magnetic entropy change

ABSTRACT

Single-phase nanocrystalline R_2Fe_{17} (R = Pr and Nd) ribbons with rhombohedral Th_2Zn_{17}-type crystalline structure (space group $R\bar{3}m$) have been fabricated by melt-spinning technique. The microstructure of the polycrystalline ribbons is composed of quasi-spherical grains with an average size below 100 nm. Transmission electron microscopy reveals that these grains are formed by agglomeration of smaller nanocrystalline entities around 15 nm in diameter, separated by disordered boundaries where the long-range crystalline order is lost. Two different ferro-to-paramagnetic phase transitions are observed, one of them coincides with that of the parent bulk alloy (290 and 326 K for R = Pr and Nd, respectively), and the other one can be ascribed to the disordered boundaries (323 and 350 K for R = Pr and Nd, respectively). For R= Pr, this fact gives rise to a significant broadening (c.a. 120 K under a magnetic field change of 2 T) of the full-width at the half-maximum of the magnetic entropy change curve, $|\Delta S_M(T)|$ (that adopts a "table-like" shape), resulting in a considerable increase of the refrigerant capacity.

1. Introduction

Stoichiometric Fe-rich R_2Fe_{17} compounds (2:17) with R = Pr and Nd crystallize in the Th_2Zn_{17}-type rhombohedral crystal structure (space group $R\bar{3}m$) where the rare-earth (R) element occupies a unique 6c crystallographic position and Fe atoms the four different 6c, 9d, 18f, and 18h sites (Wyckoff notation) [1]. As in all the rare-earth (R) transition metal (TM) compounds, their intrinsic magnetic properties are determined by the coexistence of 4f and 3d magnetism in which interatomic distances play a crucial role in both the strength and nature of R-R, R-Fe, and Fe-Fe magnetic interactions [2–4]. In particular, the magnetic coupling between Fe magnetic moments depends strongly on the Fe-Fe interatomic distance d_i [5]; it is parallel (ferromagnetic) or antiparallel (antiferromagnetic) for d_i values above or below 2.45 Å, respectively [6,7]. Despite the dominant ferromagnetic interactions, the Fe atoms located at 6c sites, which lie along the c-axis forming the so-called *"dumbbell sites"*, could couple antiferromagnetically because the Fe-Fe distances are around 2.45 Å [8,9]. The observed significant magnetovolume effects, characterized by the anomalous thermal expansion below the magnetic ordering temperature, T_C, is another consequence of the notable dependence of exchange interaction upon Fe-Fe distances [6,7,10,11]. Modified R_2Fe_{17} compounds by adding light elements (such as H, C, and N) as interstitial atoms or other transition metals with larger atomic radii than that of Fe as substitutional atoms, that provoke a lattice expansion along the crystallographic c-axis, is perhaps the best example of the effect that Fe-Fe distances have on magnetization, magnetocrystalline anisotropy, and specifically on the Curie temperature T_C [12].

These binary compounds with either Pr or Nd as rare-earth elements show a collinear ferromagnetic structure where the main contribution to the spontaneous magnetization and the magnetic ordering temperature stems from Fe atoms that exhibit a magnetic moment close to that of pure Fe, i.e., ~ 2 μ_B/Fe atom [2,13]. As for R atoms, they contribute substantially to the magnetocrystalline anisotropy in both compounds [14], and the easy magnetization direction lies along the basal plane. Pr_2Fe_{17} and N_2Fe_{17} show a high spontaneous magnetization [164.7

* Corresponding authors at: Departamento de Física, Universidad de Oviedo, Calvo Sotelo 18, 33007 Oviedo, Spain.
E-mail addresses: pgorria@uniovi.es (P. Gorria), jose.sanchez@ipicyt.edu.mx (J.L. Sánchez Llamazares).

https://doi.org/10.1016/j.jallcom.2024.173575
Received 20 October 2023; Received in revised form 10 January 2024; Accepted 15 January 2024
Available online 17 January 2024

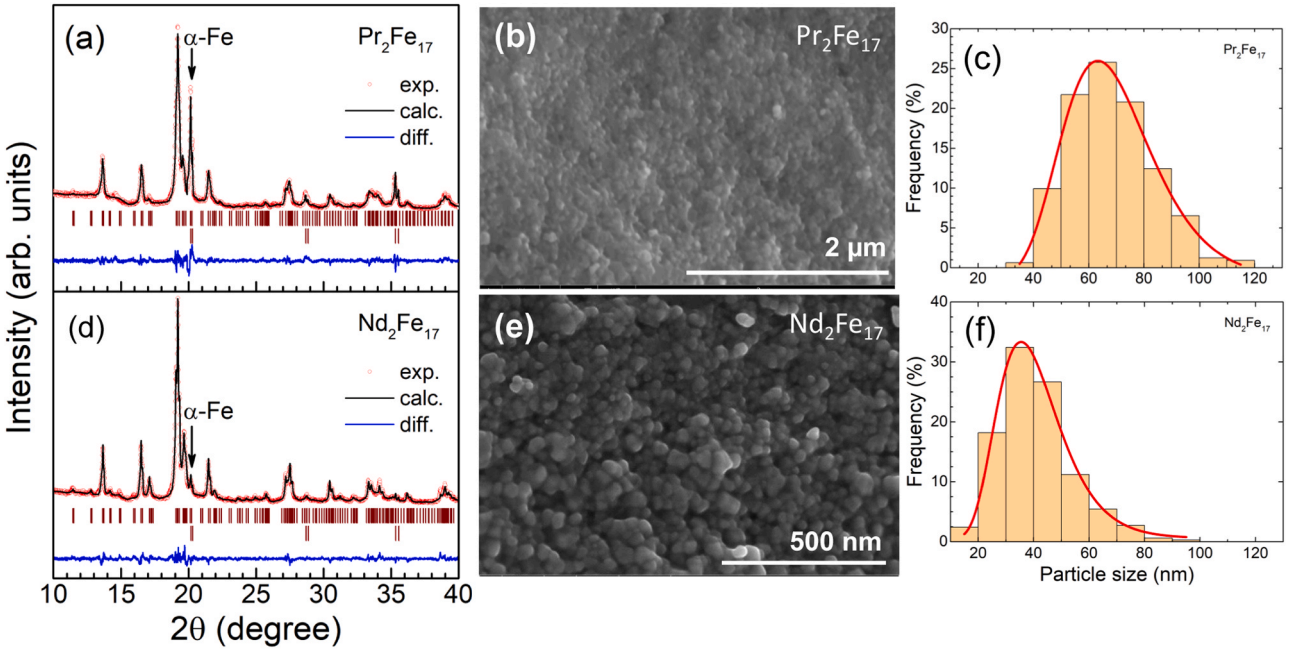

Fig. 1. Experimental (dots) and calculated (black lines) X-ray powder diffraction patterns, SEM micrographs showing the granular microstructure at the ribbon cross-section and the corresponding histograms of the particle size for Pr_2Fe_{17} [(a), (b) and (c)] and Nd_2Fe_{17} [(d), (e) and (f)] melt-spun ribbons. The vertical bars in (a) and (d) denote the Bragg positions for the rhombohedral Th_2Zn_{17}-type crystal structure, whereas the bottom blue line represents the difference between the experimental and calculated patterns.

Am^2kg^{-1} (36.3 μ_B/f.u.) and 166.7 Am^2kg^{-1} (37.0 μ_B/f.u.), for Pr and Nd, respectively] [2,4,14], and a value of T_C close to room temperature (285–295 and 326–350 K, for Pr and Nd, respectively) [2,4,14]. Both compounds display a moderate second-order magnetocaloric effect (MCE) with maximum magnetic entropy change $|\Delta S_M|^{max}$ values of ~ 6 $Jkg^{-1}K^{-1}$ for a magnetic field change $\mu_0\Delta H$ of 5 T [15–17]. However, even though they do not show a competitive adiabatic temperature change value in comparison with Gd or those materials exhibiting first-order magnetostructural transitions, the reversible nature of the effect and the low rare-earth content (< 25 wt%) have placed them in the list of potential candidates for room-temperature (RT) magnetic refrigeration applications [18].

Moreover, melt-spinning is an out-of-equilibrium fabrication technique allowing the production of many families of R-TM intermetallic alloys with different compositions in a one-step procedure [19,20]. The rapid solidification (≈ 10^6 K/min) occurring during the melt-spinning process gives rise to peculiar microstructures of the formed alloys, such as amorphous, nanocrystalline, or a mixture of both, which are not accessible by conventional arc melting or induction techniques.

In the present work, we investigate the influence of the microstructure on the magnetic and magnetocaloric properties of Pr_2Fe_{17} and Nd_2Fe_{17} thin ribbons fabricated by the melt spinning technique. The as-cast ribbons are single-phase alloys with a microstructure composed of nanocrystalline grains surrounded by disordered intergranular regions that play an essential role in the magnetic behavior of these alloys. The results are compared with those reported for the parent bulk alloys [17, 21–24].

2. Experimental methods

Fe 99.9%, Nd 99.9%, and Pr 99.98%, provided by Sigma-Aldrich, were used as raw materials to produce Pr_2Fe_{17} and Nd_2Fe_{17} ingots through arc-melting under an inert Ar atmosphere in a model MAM-1 system (from Edmund Bühler GmbH). The ingots were the precursors to obtain rapidly solidified ribbon flakes by melt spinning technique at a linear speed of the rotating copper wheel of 20 m/s. The dimensions of the ribbon flakes were typically 1–2 cm long, 1.0–1.5 mm wide, and 18–25 μm thick (determined from Scanning Electron Microscopy, SEM, observation of the cross-section). The process was carried out under a high-purity argon atmosphere in a model SC melt spinner system from Edmund Bühler GmBH.

X-ray powder diffraction (XRD) patterns of the samples were collected at room temperature in the 2θ range 10–40° with a 2θ angle step of 0.01° using Mo K_α radiation (λ_1 = 0.7093 Å, λ_2 = 0.7136 Å). For this purpose, a Seifert XRD 3000TT X-ray diffractometer in Bragg-Brentano geometry was used. The ribbons were finely powdered using an agate mortar to guarantee a random distribution and homogeneous sizes of the powders. The diffractograms were analyzed through the Le Bail and Rietveld methods using the FullProof suite package [25]. Microstructure and elemental chemical composition were investigated using a Dual Beam (FIB/SEM) FEI-Helios Nanolab 600 scanning electron microscope equipped with an energy dispersive spectroscopy (EDS) system. The nanostructure of the samples was examined in a model JEM-2100 F field emission high-resolution transmission electron microscope (HRTEM). Several HRTEM images at different resolution scales of small ribbon particles deposited on carbon-coated TEM grids were collected for each sample. With such a purpose, ribbon samples were finely pulverized, poured into a vial with ethanol, and sonicated for 10 min in an ultrasonic bath to form a suspension. Drops taken from its upper part were deposited into the TEM grids and carefully dried. SEM and HRTEM images were analyzed using ImageJ software [26].

Magnetization as a function of temperature T and applied magnetic field μ_0H, i.e., $M(T)$ and $M(\mu_0H)$ curves, were measured by vibrating sample magnetometry in a Quantum Design PPMS® Dynacool®−9 T platform. $M(T)$ curves were recorded at a 1.0 K/min T sweep rate. The magnetic transition temperatures were obtained from the minimum of the first temperature derivative of the $M(T)$ curves measured under a magnetic field of 5 mT. The temperature dependence of the magnetic entropy change $|\Delta S_M(T)|$ was determined numerically by integrating the Maxwell relation from the sets of $M(\mu_0H)$ curves shown in Fig. 4a, c.

3. Results and discussion

Fig. 1(a), (d) show the experimental and calculated XRD patterns for

Table 1
Crystal structure and microstructure data, saturation magnetization M_S at 2 K and 5 T, and Curie temperature T_C determined from the low-field $M(T)$ curves for Pr_2Fe_{17} and Nd_2Fe_{17} alloy ribbons. The results are compared with previous data reported for bulk alloys [21,23].

Material	Pr_2Fe_{17} ribbons	Pr_2Fe_{17} bulk*	Nd_2Fe_{17} ribbons	Nd_2Fe_{17} bulk* *
a (Å)	8.5586(3)	8.5849	8.5679(2)	8.582(1)
c (Å)	12.523(1)	12.4659	12.462(1)	12.463(1)
c/a	1.463(4)	1.452(3)	1.455(4)	1.452(3)
V (Å^3)	794.38(7)	795.66	792.23(3)	795
Fe-Fe (6c) (Å)	2.422(3)	2.411(2)	2.410(3)	2.410(2)
χ^2	3.3	7.0	3.2	1.3
R_B (%)	4.9	3.3	6.6	5.8
Fe (% wt.)	3.7	7.2	1.0	3.0
<d> (nm)	70	-	41	-
$<\tau>$ (nm)	15	-	12	-
M_S (Am^{2}kg^{-1})	159	162	147	138
T_C (K)	290, 323	286 ± 1	326, 350	339 ± 5

powdered samples of both compounds. The values for the unit cell parameters and the cell volume, together with the reliability factors of the fits, are given in Table 1. For comparison, the table also displays the data available for bulk alloys. The fitting of both patterns reveals that as-cast ribbon samples crystallize into the Th_2Zn_{17}-type rhombohedral crystal structure (space group $R\bar{3}m$) with a cell volume slightly reduced (≈ 0.2%) compared to the reported for bulk and high-energy-ball milled (HEBM) alloys. Moreover, the Bragg peaks' broadening suggests small nanometer length-scale crystallite sizes. A small amount of α-Fe impurities has been detected, as can be deduced from the presence of the (110) Bragg reflection, marked with a vertical arrow in Fig. 1(a), (d). However, the amount of such impurities estimated from the Rietveld fitting, 3.7 and 1.0 wt% for Pr_2Fe_{17} and Nd_2Fe_{17} ribbons, respectively, is well below the percentages found for HEBM powders (around 7 wt%) [21,23]. It is worth noting that no traces of iron oxides and/or rare-earth oxides were found. In Table 1, the relevant Fe-Fe distances for the dumbbell-pairs (6c site) are included for easy comparison, being around 2.4 Å.

The SEM images of the ribbon cross-section [see Fig. 1(b), (e)] show a typical granular morphology, consisting of quasi-spherical

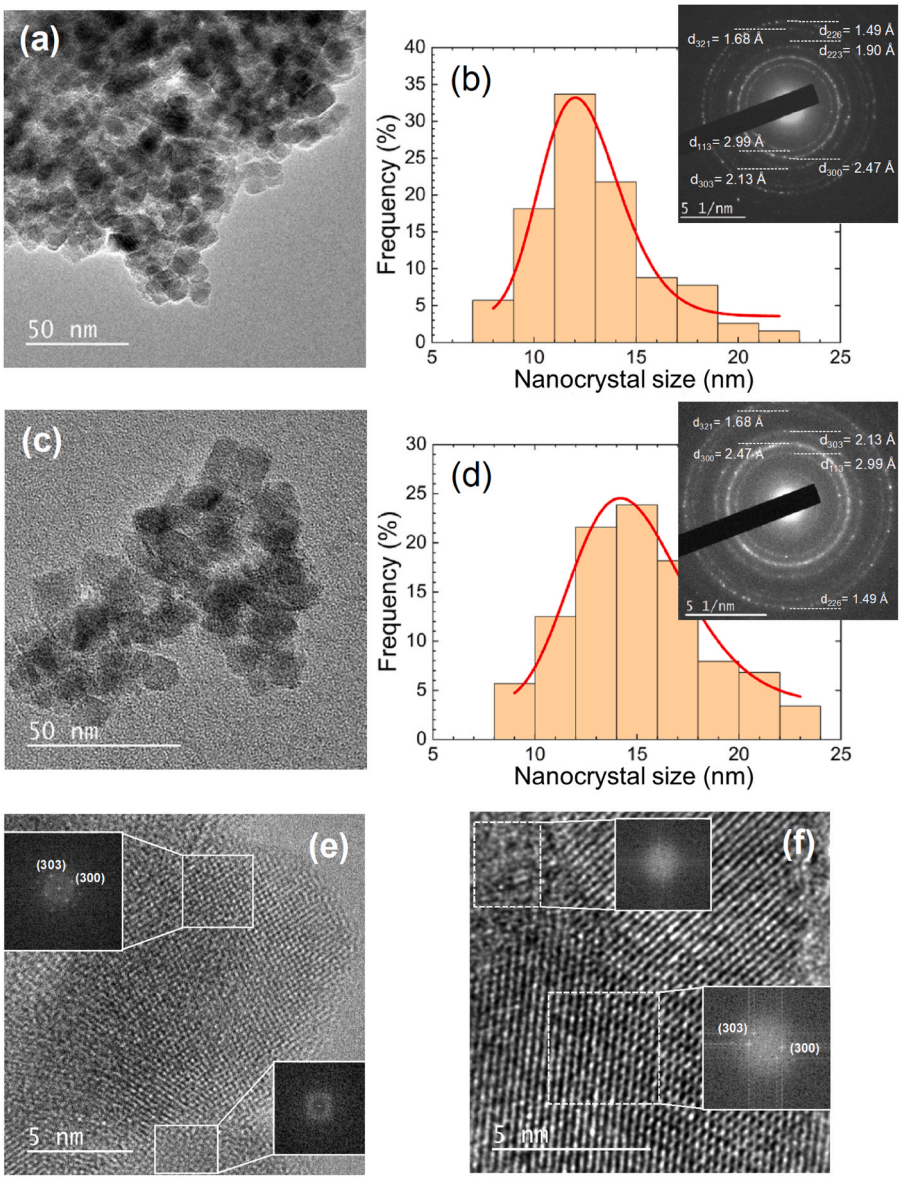

Fig. 2. Typical high-resolution TEM images and histograms of the nanocrystal size distribution for Pr_2Fe_{17} [(a) and (b)] and Nd_2Fe_{17} [(c) and (d)] melt-spun ribbons. The inset in (b) and (d) shows the selected area electron diffraction (SAED) pattern of the respective TEM images. (e) and (f) show the Fourier transform of a nanocrystal and the disordered intergranular phase for Pr_2Fe_{17} and Nd_2Fe_{17} ribbons.

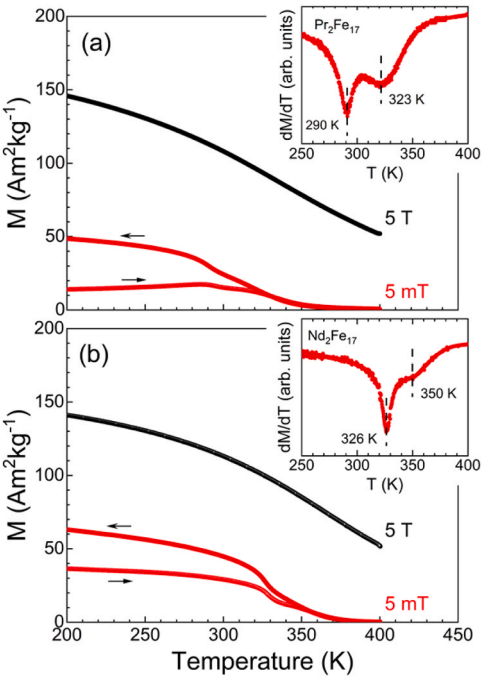

Fig. 3. Thermomagnetic curves measured under static magnetic fields at 5 mT and 5 T for Pr_2Fe_{17} (b) and Nd_2Fe_{17} (b) melt-spun ribbons. The insets show the temperature dependence of the first derivative of magnetization at 5 mT in the temperature interval of the ferromagnetic transition.

polycrystalline grains, but unusually small in size (tens of nanometers) compared with other polycrystalline melt-spun intermetallic RE-TM ribbons in which the average grain size is of the order of 1 μm [27]. From the fit of the histograms obtained after counting more than 300 grains [see Fig. 1(c), (f)] to a log-normal distribution, the average size <d> for these grains are 70 and 41 nm for Pr_2Fe_{17} and Nd_2Fe_{17} ribbons, respectively. Despite the solidification process occurring under a high thermal gradient, which is predominantly perpendicular to the ribbons' plane, samples do not show preferential grain growth (i.e., they seem to be isotropic). Several TEM and HRTEM images were collected for both ribbon samples to assess the grains' morphology better. The images shown in Fig. 2(a), (c) reveal that each of such grains is indeed an agglomeration of smaller nanocrystals with an average size, $<\tau(\sigma)> =$ 15(3) and 12(2) nm for Pr_2Fe_{17} and Nd_2Fe_{17}, respectively, estimated from the log-normal fit of the histograms shown in Fig. 2(b), (d). These values are in good agreement with those obtained from the Rietveld fit of the x-ray diffraction patterns (around 20 nm). Thus, SEM and TEM images unveil a markedly two-scale microstructure of the ribbons. Moreover, the analysis of several diffraction rings in the selected area electron diffraction (SAED) patterns confirms the Th_2Zn_{17}-type rhombohedral crystal structure [see insets in Fig. 2(b), (d) where the Miller indices corresponding to some lattice d-spacings are depicted].

In the HRTEM images of Fig. 2(e), (f) obtained at higher magnification, we show an individual nanocrystal surrounded by a lighter gray region where the absence of ordered atomic layers is recognizable. This a quite common in melt-spun magnetic ribbons, where it is likely to find a dual microstructure with different atomic arrangements and, consequently, different magnetic properties, such as saturation magnetization, coercivity, or Curie temperature (see below). The insets in Fig. 2(e), (f) show the typical Fourier transform (FT) patterns of individual nanocrystals (upper insets) and their surrounding disordered region (bottom insets). Whereas some diffraction spots are identified in the FT patterns inside the nanocrystalline region, only typical "amorphous haloes" are observed in the FT patterns of the regions surrounding the nanocrystals, thus confirming the absence of long-range atomic order within these regions. Another feature that evidences the existence of a disordered phase comes from the low-angle region of the diffraction patterns (see Fig. 1(a), (d), where an increase of the background signal can be perceived (below 16º). Hence, we can conclude that at the nanometer length scale, two phases coexist with the same composition but different structures, nanocrystals surrounded by a disordered or amorphous-like region.

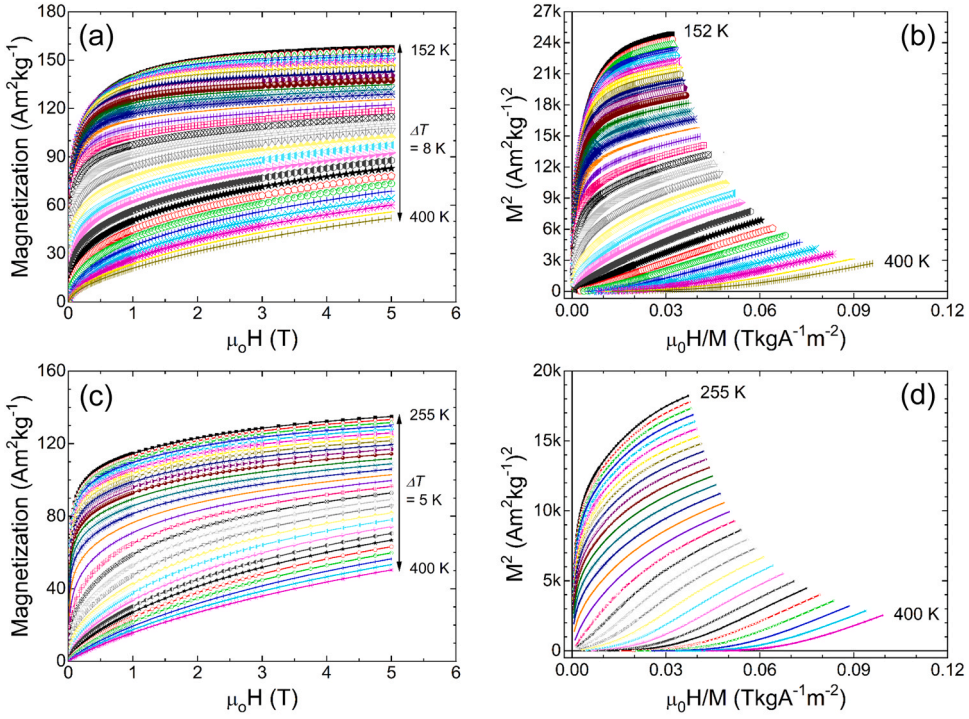

Fig. 4. Set of isothermal magnetization $M(\mu_oH)$ curves across the second-order magnetic phase transition and Arrott plots (i.e., M^2 vs. μ_oH/M) for Pr_2Fe_{17} [(a) and (b)] and Nd_2Fe_{17} [(c) and (d)].

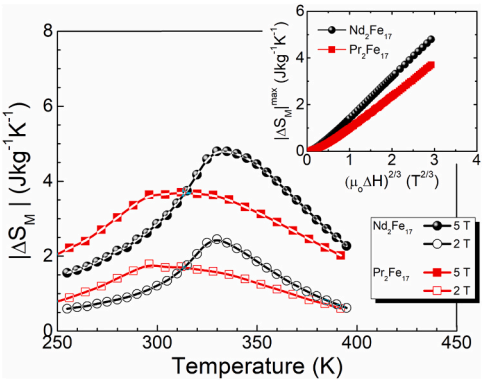

Fig. 5. Temperature dependence of the isothermal magnetic entropy change under $\mu_0\Delta H = 2$ and 5 T for Pr_2Fe_{17} and Nd_2Fe_{17} melt-spun ribbons. The inset shows the $|\Delta S_M|^{max}$ versus $(\mu_0\Delta H)^{2/3}$ dependencies.

Fig. 3(a), (b) show the temperature dependence of the magnetization, $M(T)$ curves, measured under low (5 mT) and high (5 T) magnetic fields, and after zero-field-cooling and field-cooling procedures for Pr_2Fe_{17} and Nd_2Fe_{17} ribbons, respectively. Firstly, we notice that the low-field $M(T)$ curves display a two-step falling of the magnetization before reaching an almost vanishing value in both samples, thus suggesting the existence of two different values of the Curie temperature, T_C. To determine those T_C values for each sample, we performed the temperature derivative of the magnetization versus temperature. In the insets of Fig. 3 (a), (b), two successive minima can be visualized: (i) a narrow and well-defined one at 290 K and 326 K for Pr_2Fe_{17} and Nd_2Fe_{17}, respectively, that match with the reported values for the T_C of the corresponding bulk alloys, and (ii) a broad minimum at 323 K and 350 K for Pr_2Fe_{17} and Nd_2Fe_{17}, respectively. Hence, we assume that (i) can be ascribed to the Curie temperature of the nanocrystalline phases T_C^{nc}, and (ii) to that of the amorphous regions surrounding the nanocrystallites T_C^{am}. Two aspects regarding T_C^{am} are interrelated and deserve further discussion. On the one hand, a broader minimum in the dM/dT vs. T curve suggests a distribution of Curie temperatures for the disordered region instead of a unique, well-defined value [28]. Moreover, there is an enhancement of the value for the Curie temperature of this amorphous region, $T_C^{am} > T_C^{nc}$, probably due to an average slight increase of the Fe-Fe interatomic distances that favors ferromagnetic exchange interactions [6,7]. Similar results involving an enhancement of the Curie temperature have been reported in the literature for Invar Fe-rich FeZr-based metallic glasses around 90% at. in Fe. Surprisingly, the addition of boron and/or zirconium, and thus a reduction in the iron content, gives rise to a noticeable increase (up to 100 K) in the value of T_C [29,30]. In addition, it has been observed that T_C can be augmented by tensile stress in FeZrB metallic glasses [31]. It seems, that in both cases a small increase in the average Fe-Fe interatomic distances is produced. As it is well-known, R_2Fe_{17} intermetallic compounds exhibit large magneto-volume coupling, the negative thermal expansion and Invar effect for temperatures below T_C being the most representative features, associated with slight variations of the distances between Fe atoms along the z-axis direction ("dumbbell-sites") [6,7,22,23,32]. Another signature for the strong magneto-volume coupling can be inferred from the $M(T)$ curves measured under a magnetic field of 5 T. As shown in Fig. 3, the magnetization exhibits a long "tail" for $T > T_C$ up to 1.2 T_C or higher, indicating the existence of moment-volume instabilities characteristic of Invar-type alloys [33].

Table 3
$|\Delta S_M|^{max}$, and *RC*-1, *RC*-2, *RC*-3, and related δT_{FWHM}, and T_{hot}, and T_{cold} values for magnetic field changes $\mu_o\Delta H$ from 1 to 5 T for Pr_2Fe_{17} melt-spun ribbons. The values of RC were estimated form the field dependence of RC in Fig. 6(a).

$\mu_o\Delta H$ (T)	1.0	2.0	3.0	4.0	5.0
$\lvert\Delta S_M\rvert^{max}$ (J kg^{-1} K^{-1})	1.0	1.8	2.5	3.1	3.7
RC-1 (J kg^{-1})	95	208	328	450	≈ 580
RC-2 (J kg^{-1})	74	163	259	357	≈ 450
δT_{FWHM} (K)	96	117	133	145	≈ 155
T_{hot} (K)	361	373	383	391	-
T_{cold} (K)	265	256	250	246	242
RC-3 (J kg^{-1})	48	105	164	228	≈ 290
δT^{RC-3} (K)	82	108	132	133	-
T_{hot}^{RC-3} (K)	353	368	382	385	-
T_{cold}^{RC-3} (K)	271	260	250	252	-

We have investigated the intrinsic and extrinsic effects that nanostructuring has on a magneto-thermal property such as the magnetocaloric effect (MCE) across the second-order ferromagnetic phase transition through the magnetization curves, $M(\mu_0 H)$, measured under magnetic field changes up to 5 T [see Fig. 4(a), (c)]. From them, we calculated the temperature dependence of the magnetic entropy change, $\Delta S_M(T)$ curves, for different magnetic field changes. Fig. 5 displays the $|\Delta S_M(T)|$ curves for $\mu_0\Delta H = 2$ and 5 T. The inset in both figures shows that $|\Delta S_M|^{max}$ linearly depends on $(\mu_0\Delta H)^{2/3}$ as expected for ferromagnetic materials across the second-order phase transition [Fig. 4(b),(d) show the Arrot plots of both samples] whose behavior obeys the mean-field theory [32].

Tables 2 and 3 summarize the most relevant information regarding the magnetocaloric properties of both ribbon samples. The $|\Delta S_M(T)|$ curves display a "caret-like" shape for the bulk alloys [17], however for Nd_2Fe_{17} ribbons, the curves show a broad maximum located at around 330 K (reaching values of $|\Delta S_M|^{max} = 2.5$ and 4.8 Jkg^{-1}K^{-1} for $\mu_0\Delta H = 2$ and 5 T, respectively), whereas for Pr_2Fe_{17} ribbons the $\Delta S_M(T)$ curve exhibit a table-like shape in the temperature range between 296 and 329 K (with $|\Delta S_M|^{max}$ values of 1.8 and 3.7 Jkg^{-1}K^{-1} for $\mu_0\Delta H = 2$ and 5 T, respectively). Therefore, it seems that a compromise between the value of $|\Delta S_M|^{max}$ and $\Delta T_C = T_C^{am} - T_C^{nc}$ is needed to achieve a table-like behavior of the $|\Delta S_M(T)|$ curve, which optimizes an Ericsson thermodynamic cycle [34] and maximizes the refrigerant capacity, *RC*, of the material. In Fig. 6 (a),(b) the dependence of the refrigerant capacity, *RC*, on the magnetic field change, obtained from the criteria established in literature, is depicted. This condition is better fulfilled in the case of R = Pr, although Nd_2Fe_{17} shows higher $|\Delta S_M|^{max}$ values. As seen from Table 4, for $\mu_0\Delta H = 2$ T, the *RC* of Pr_2Fe_{17} ribbons is substantially enhanced (almost 50%) compared to that of the bulk alloy and is about 25% higher than that of Nd_2Fe_{17} ribbons and other reported values for bulk Nd_2Fe_{17}-based alloys [23,24,38]. It is worth noting that the estimated value for RC-1 in Pr_2Fe_{17} ribbons for $\mu_0\Delta H = 5$ T (Fig. 6a and Table 3) is approximately the same to that reported for ball-milled powders, and slightly higher than that of bulk alloy [17,39] and other $Pr_2Fe_{17-x}M_x$ pseudo-binary intermetallics with Al [39], Mn [40] or Ni [41].

Table 2
$|\Delta S_M|^{max}$, *RC*-1, δT_{FWHM}, T_{hot}, and T_{cold} under $\mu_0\Delta H = 1.5$ T for Pr_2Fe_{17} and Nd_2Fe_{17} melt-spun ribbons and their mechanical milled and bulk counterparts [21,24].

	Pr_2Fe_{17} ribbons	Pr_2Fe_{17} bulk*	Pr_2Fe_{17} (MM 10 h)*	Nd_2Fe_{17} ribbons	Nd_2Fe_{17} bulk* *	Nd_2Fe_{17} (MM 10 h)**
$\lvert\Delta S_M\rvert^{max}$ (J kg^{-1} K^{-1})	1.4	2.6	2.1	2.0	2.6	1.9
RC-1 (J kg^{-1})	149	105	107	118	122	130
δT_{FWHM} (K)	107	40	51	61	47	70
T_{hot} (K)	261	265	252	303	315	304
T_{cold} (K)	368	305	303	364	362	374

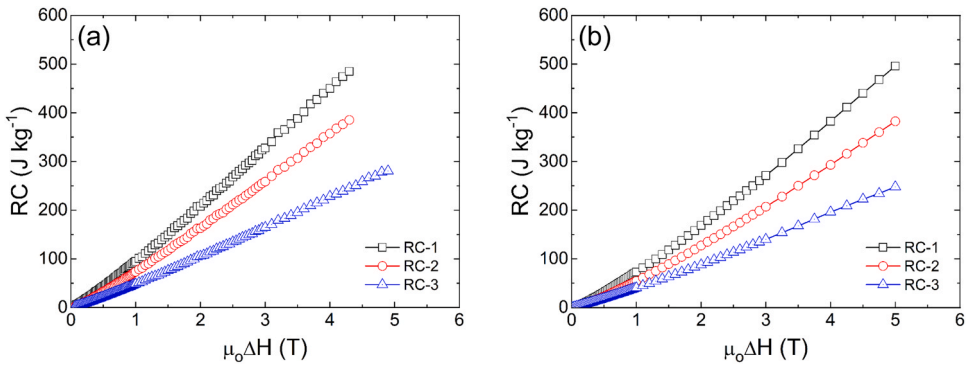

Fig. 6. Magnetic field change dependence of *RC*-1, *RC*-2, and *RC*-3 refrigerant capacities for nanostructured Pr_2Fe_{17} (a) and Nd_2Fe_{17} (b) ribbons [35–37].[1]

Table 4
$|\Delta S_M|^{max}$, and *RC*-1, *RC*-2, *RC*-3, and related δT_{FWHM}, and T_{hot}, and T_{cold} values, for magnetic field changes $\mu_o\Delta H$ from 1 to 5 T for Nd_2Fe_{17} melt-spun ribbons.

$\mu_o\Delta H$ (T)	1.0	2.0	3.0	4.0	5.0
$\lvert\Delta S_M\rvert^{max}$ (J kg^{-1} K^{-1})	1.4	2.5	3.3	4.1	4.8
RC-1 (J kg^{-1})	73	169	271	382	496
RC-2 (J kg^{-1})	55	127	207	293	382
δT_{FWHM} (K)	52	68	82	93	103
T_{hot} (K)	358	369	378	386	392
T_{cold} (K)	306	301	296	293	289
RC-3 (J kg^{-1})	40	88	140	196	248
$\delta T^{RC\text{-}3}$ (K)	105	115	112	116	103
T_{hot}^{RC-3} (K)	378	388	391	395	392
T_{cold}^{RC-3} (K)	273	273	279	279	289

Thus, the heavy rare earths with high total angular momentum, J, and their intermetallic compounds are therefore preferential choices for room temperature magnetic refrigerants, and still today ensures further investigations on the different magnetic-thermal properties of these R_2Fe_{17} alloys.

4. Final remarks

In summary, we would like to emphasize that the relevance of a current investigation is to obtain through a one-step fabrication method, like melt-spinning, R_2Fe_{17} (R = Pr and Nd) single-phase ribbons with a mixed microstructure (nanocrystalline/amorphous). The appropriate combination of the magnetic phase transition temperatures related to the ordered (nanocrystalline) and disordered (amorphous) regions in the sample and the magnitude of the corresponding isothermal magnetic entropy change lead to a table-like shape of the $|\Delta S_M(T)|$ curve of the Pr-based alloy. In addition, a remarkable improvement of the refrigerant capacity is achieved for the ribbon samples compared with the parent bulk alloy (over 40% larger for a magnetic field change of 2 T).

CRediT authorship contribution statement

C.F. Sanchez-Valdes: Writing – review & editing, Writing – original draft, Validation, Software, Investigation, Funding acquisition, Formal analysis. **J.A. Blanco:** Writing – review & editing, Writing – original draft, Visualization, Funding acquisition. **J.L. Garrido-Alvarez:** Writing – original draft, Software, Investigation, Formal analysis. **P. Alvarez-Alonso:** Writing – review & editing, Methodology, Investigation, Formal analysis, Data curation. **Pedro Gorria:** Writing – review & editing, Writing – original draft, Visualization, Validation, Investigation, Funding acquisition, Formal analysis, Data curation. **J.L. Sanchez Llamazares:** Writing – review & editing, Visualization, Validation, Supervision, Methodology, Investigation, Data curation, Conceptualization.

Declaration of Competing Interest

The authors declare that they have no known competing financial interests or personal relationships that could have appeared to influence the work reported in this paper.

Data Availability

Data will be made available on request.

Acknowledgments

We want to express our recognition and gratitude to Prof. V.K. Pecharsky for his always enthusiastic scientific comments and discussions everytime we met him. Beyond the laboratory, Prof. Pecharsky's warm personality and honest interest in the well-being of his colleagues created a feeling of community and camaraderie. His ability to bridge the gap between professionalism and personal connection made him not only a respected mentor but also a cherished friend. This work was supported by SEP-CONAHCyT, Mexico (research grant A1-S-37066), Laboratorio Nacional de Nanociencias y Nanotecnologia (LINAN, IPICyT), Spanish AEI agency, MCI, & EU FEDER (project Ref.: PID2022–138256NB-C21) and Asturian government (project number: SV-PA-21-AYUD/2021/51822). Authors acknowledge the technical support received from LINAN's personnel, M.Sc. B.A. Rivera-Escoto, M. Sc. A.I. Peña-Maldonado, and Dr. I.G. Becerril-Juárez, during the development of this investigation. J.L. Sánchez Llamazares acknowledges the support received from the European Union-NextGenerationEU, Ministerio de Universidades, and Plan de Recuperación, Transformación y Resiliencia, in the framework of the Maria Zambrano program of the University of Oviedo, Asturias, Spain (Reference: MU-21-UP2021–030 71741542). C.F. Sánchez-Valdés is grateful to UACJ for supporting his sabbatical research stay at Universidad de Oviedo. Authors would like to acknowledge the technical support provided by Dr. Martinez-Blanco (Servicios Científico-T é cnicos de la Universidad de Oviedo).

References

[1] Q. Johnson, D.H. Wood, G.S. Smith, A.E. Ray, Q. Johnson, Refinement of Th_2Zn_{17} structure: Pr_2Fe_{17}, Acta Cryst. B24 (1968) 274–276, https://doi.org/10.1107/S0567740868002086.
[2] K.H.J. Buschow, Intermetallic compounds of rare-earth and 3d transition metals, Rep. Prog. Phys. 40 (1977) 1179, https://doi.org/10.1088/0034-4885/40/10/002.

[1] Criteria used to estimate *RC*-1, *RC*-2, and *RC*-3: (a) *RC*-1 = $|\Delta S_M|^{max} \times (T_{hot} - T_{cold})$, where T_{hot} and T_{cold} are the temperatures defining the temperature interval of the full width at half-maximum of the $\Delta S_M(T)$ curve δT_{FWHM} (i.e., $\delta T_{FWHM} = T_{hot} - T_{cold}$); (b) *RC*-2 = $\int_{T_{cold}}^{T_{hot}} |\Delta S_M(T)|\,dT$, and; (c) *RC*-3 is given the maximum rectangular area that can be inscribed below the $|\Delta S_M(T)|$ curve.[35–37]

[3] K.H.J. Buschow, Rare Earth Compounds, chapter 4, in Ferromagnetic Materials, vol. 1, E.P. Wohlfarth (Editor), Amsterdam: North-Holland, pp. 297–414, 1980. https://doi.org/10.1016/S1574–9304(05)80119–1.

[4] J.J.M. Franse, R.J. Radwanski, Magnetic Properties of Binary Rare-earth 3d-transition-metal Intermetallic Compounds, chapter 5, in Handbook of Magnetic Materials, Vol. 7, K.H.J. Buschow (Editor), Elsevier Science Publishers B.V., Amsterdam 1993, pp. 307–501. https://doi.org/10.1016/S1567–2719(05)80046–0.

[5] K.H.J. Buschow, Magnetic interactions in intermetallic compounds, J. Less-Common Met. 43 (1975) 55, https://doi.org/10.1016/0022-5088(75)90123-X.

[6] D. Givord, W. James, J.M. Moreau, R. Lemaire, J. Shah, Magnetic behavior of rare-earth iron-rich intermetallic compounds, IEEE Trans. Magn. 7 (1971) 657, https://doi.org/10.1109/TMAG.1971.1067051.

[7] D. Givord, R. Lemaire, Magnetic transition and anomalous thermal expansion in R_2Fe_{17} compounds, IEEE Trans. Magn. 10 (1974) 109–113, https://doi.org/10.1109/TMAG.1974.1058311.

[8] G.J. Long, O.A. Pringle, F. Grandjean, W.B. Yelon, K.H.J. Buschow, A neutron diffraction and Mössbauer effect study of the magnetic properties of Pr_2Fe_{17} and $Pr_2Fe_{17}N_{2.6}$, J. Appl. Phys. 74 (1993) 504, https://doi.org/10.1063/1.355261.

[9] Z.W. Li, X.Z. Zhou, A.H. Morrish, Site occupancies of Si atoms and curie temperatures for $Sm_2Fe_{17-x}Si_x$, Phys. Rev. B 51 (1995) 2891, https://doi.org/10.1103/PhysRevB.51.2891.

[10] Z. Arnold, J. Kamarád, L. Morellón, M.R. Ibarra, Magnetovolume effects and anomalous compressibility of Nd_2Fe_{17} and $Nd_2(FeTi)_{17}$ compounds, J. Appl. Phys. 81 (1997) 5693, https://doi.org/10.1063/1.364903.

[11] M. Brouha, K.H.J. Buschow, A.R. Miedema, Magneto-volume effects in rare-earth transition metal intermetallics, IEEE Trans. Magn. 10 (1974) 182, https://doi.org/10.1109/TMAG.1974.1058330.

[12] H. Fujii, H. Sun, Interstitially Modified Intermetallics of Rare Earth and 3D Elements, chapter 3, in Handbook of Magnetic Materials, Elsevier, Vol. 9, pp. 303–404, ISSN 1567–2719, ISBN 9780444822321, 1995. https://doi.org/10.1016/S1567–2719(05)80007–1.

[13] F. Weitzer, K. Hiebl, P.J. Rogl, Al, Ga substitution in RE_2Fe_{17} (RE= Ce, Pr, Nd): magnetic behavior of $RE_2Fe_{15}(Al, Ga)_2$ alloys, J. Appl. Phys. 65 (1989) 4963, https://doi.org/10.1063/1.343218.

[14] X.C. Kou, F.R. de Boer, R. Grossinger, G. Wiesinger, H. Suzuki, H. Kitazawa, T. Takamasu, G. Kido, Magnetic anisotropy and magnetic phase transitions in R_2Fe_{17} with R = Y, Ce, Pr, Nd, Sm, Gd, Tb, Dy, Ho, Er, Tm and Lu, J. Magn. Magn. Mater. 177 (1998) 1002, https://doi.org/10.1016/S0304-8853(97)00798-1.

[15] S.Y. Dan'kov, V.V. Ivtchenko, A.M. Tishin, K.A. Gschneidner, Jr, V.K. Pecharsky, Magnetocaloric effect in $GdAl_2$ and Nd_2Fe_{17}, Adv. Cryog. Eng. 46 (2000) 397, https://doi.org/10.1007/978-1-4615-4293-3_51.

[16] K. Mandal, A. Yan, P. Kerschl, A. Handstein, O. Gutfleisch, K.-H. Müller, The study of magnetocaloric effect in R_2Fe_{17} (R = Y, Pr) alloys, J. Phys. D Appl. Phys. 37 (2004) 2628, https://doi.org/10.1088/0022-3727/37/19/002.

[17] P. Gorria, J.L. Sánchez Llamazares, P. Álvarez-Alonso, M.J. Pérez, J. Sánchez Marcos, J.A. Blanco, Relative cooling power enhancement in magneto-caloric nanostructured Pr_2Fe_{17}, J. Phys. D Appl. Phys. 41 (Issue 19) (2008) 192003, https://doi.org/10.1088/0022-3727/41/19/192003.

[18] J. Liu, T. Gottschall1, K.P. Skokov, J.D. Moore, Oliver Gutfleisch, Giant magnetocaloric effect driven by structural transitions, Nat. Mater. 11 (2012) 620, https://doi.org/10.1038/NMAT3334.

[19] J.L. Sánchez Llamazares, P. Álvarez-Alonso, C.F. Sánchez-Valdés, P.J. Ibarra-Gaytán, J.A. Blanco, P. Gorria, Investigating the magnetic entropy change in single-phase Y_2Fe_{17} melt-spun ribbons, Curr. Appl. Phys. 16 (2016) 963–968, https://doi.org/10.1016/j.cap.2016.05.013.

[20] C.F. Sánchez-Valdés, P. Ibarra-Gaytán, J.L.S.ánchez Llamazares, M. Ávalos-Borja, P. Álvarez-Alonso, P. Gorria, J.A. Blanco, Enhanced refrigerant capacity in two-phase nanocrystalline/amorphous $NdPrFe_{17}$ melt-spun ribbons, Appl. Phys. Lett. 104 (2014) 15–20, https://doi.org/10.1063/1.4879544.

[21] J.L. Sánchez Llamazares, M.J. Pérez, P. Álvarez, J.D. Santos, M.L. Sánchez, B. Hernando, J.A. Blanco, P. Gorria, The effect of ball milling in the microstructure and magnetic properties of Pr_2Fe_{17} compound, J. Alloy. Compd. 483 (2009) 682–685, https://doi.org/10.1016/j.jallcom.2008.07.210.

[22] P. Gorria, P. Álvarez, J. Sánchez Marcos, J.L. Sánchez Llamazares, M.J. Pérez, J. A. Blanco, Crystal structure, magnetocaloric effect and magnetovolume anomalies in nanostructured Pr_2Fe_{17}, Acta Mater. 57 (2009) 1724–1733, https://doi.org/10.1016/j.actamat.2008.12.014.

[23] P. Álvarez, P. Gorria, V. Franco, J.S. Marcos, M.J. Pérez, J.L. Sánchez Llamazares, I. Puente Orench, J.A. Blanco, Nanocrystalline Nd_2Fe_{17} synthesized by high-energy ball milling: crystal structure, microstructure and magnetic properties, J. Phys. Condens. Matter 22 (2010) 216005, https://doi.org/10.1088/0953-8984/22/21/216005.

[24] P. Álvarez, J. Sánchez Marcos, J.L. Sánchez Llamazares, V. Franco, M. Reiffers, J. A. Blanco, P. Gorria, Magnetocaloric effect in nanostructured Pr_2Fe_{17} and Nd_2Fe_{17} synthesized by high-energy ball-milling, Acta Phys. Pol. A 118 (2010) 867, https://doi.org/10.12693/APhysPolA.118.867.

[25] J. Rodríguez-Carvajal, Recent advances in magnetic structure determination by neutron powder diffraction, Phys. B 192 (1993) 55–69, https://doi.org/10.1016/0921-4526(93)90108-I.

[26] C.T. Rueden, J. Schindelin, M.C. Hiner, B.E. DeZonia, A.E. Walter, E.T. Arena, K. W. Eliceiri, ImageJ2: imageJ for the next generation of scientific image data, BMC Bioinform. 18 (2017) 529, https://doi.org/10.1186/s12859-017-1934-z.

[27] C. Chen, S. Kodat, M. Walmer, S. Cheng, M. Willard, V. Harris, Effects of grain size and morphology on the coercivity of $Sm_2(Co_{1-x}Fe_x)_{17}$ based powders and spin cast ribbons, J. Appl. Phys. 93 (2003) 7966–7968, https://doi.org/10.1063/1.1558272.

[28] P. Alvarez-Alonso, J.L. Sánchez Llamazares, C.F. Sánchez-Valdés, G.J. Cuello, V. Franco, P. Gorria, J.A. Blanco, On the broadening of the magnetic entropy change due to Curie temperature distribution, J. Appl. Phys. 115 (2014) 17A929, https://doi.org/10.1063/1.4867346.

[29] J.M. Barandiarán, P. Gorria, I. Orúe, M.L. Fernández-Gubieda, F. Plazaola, J. C. Gómez Sal, L. Fernández Barquín, L. Fournes, Magnetic and transport properties of Fe - Zr - B - (Cu) amorphous alloys, J. Phys. Condens. Matter. 9 (1997) 5671, https://doi.org/10.1088/0953-8984/9/26/014.

[30] L. Fernández Barquín, J.C. Gómez Sal, P. Gorria, J.S. Garitaonandia, J. M. Barandiarán, Dynamic susceptibility of reentrant Fe-rich inhomogeneous amorphous alloys, Eur. Phys. J. B 35 (3) (2003), https://doi.org/10.1140/epjb/e2003-00250-0.

[31] J.M. Barandiarán, P. Gorria, I. Orúe, M.L. Fdez-Gubieda, F. Plazaola, A. Hernando, Tensile stress dependence of the Curie temperature and hyperfine field in Fe-Zr-B-(Cu) amorphous alloys, Phys. Rev. B 54 (1996) 3026, https://doi.org/10.1103/PhysRevB.54.3026.

[32] P. Álvarez-Alonso, P. Gorria, J.A. Blanco, J. Sánchez-Marcos, G.J. Cuello, I. Puente-Orench, J.A. Rodríguez-Velamazán, G. Garbarino, I. de Pedro, J.R. Fernández, J. L. Sánchez Llamazares, Magnetovolume and magnetocaloric effects in Er_2Fe_{17}, Phys. Rev. B 86 (2012) 184411, https://doi.org/10.1103/PhysRevB.86.184411.

[33] E.F. Wasserman, Invar: moment-volume instabilities in transition metals and alloys in, Ferromagn. Mater. vol. 5 (1990) 237–322, https://doi.org/10.1016/S1574-9304(05)80063-X.

[34] P. Álvarez-Alonso, P. Gorria, J.L. Sánchez-Llamazares, J.A. Blanco, Searching the conditions for a table-like shape of the magnetic entropy in magneto-caloric materials, J. Alloy. Compd. 568 (2013) 98–101, https://doi.org/10.1016/j.jallcom.2013.03.105.

[35] A.M. Tishin, Y.I. Spichkin. The Magnetocaloric Effect and its Applications, IOP, Bristol, 2003.

[36] M.E. Wood, W.H. Potter, General analysis of magnetic refrigeration and its optimization using a new concept: maximization of refrigerant capacity, Cryogenics 25 (1985) 667, https://doi.org/10.1016/0011-2275(85)90187-0.

[37] K.A. Gschneidner Jr, V.K. Pecharsky, A.O. Pecharsky, C.B. Zimm, Recent developments in magnetic refrigeration, Mater. Sci. Forum 315-317 (1999) 69, https://doi.org/10.4028/www.scientific.net/MSF.315-317.69.

[38] W. Bouzidi, K. Nouri, T. Bartoli, R. Sedek, H. Lassri, J. Moscovici, L. Bessais, Study of the magnetic and magnetocaloric properties at low-field in $Nd_2Fe_{17-x}Si_x$ Intermetallics, J. Magn. Magn. Mater. 497 (2020) 166018.

[39] R. Guetari, R. Bez, A. Belhadj, K. Zehani, A. Bezergheanu, N. Mliki, L. Bessais, C. B. Cizmas, Influence of Al substitution on magnetocaloric effect of $Pr_2Fe_{17-x}Al_x$, J. Alloy. Compd. 588 (2014) 64–69, https://doi.org/10.1016/j.jallcom.2013.10.184.

[40] X.-C. Zhong, Z.-W. Liu, D.-C. Zeng, K.A. Gschneidner Jr, V.K. Pecharsky, Magnetocaloric effect of $Pr_2Fe_{17-x}Mn_x$ alloys, Rare Met. 33 (2014) 552–555, https://doi.org/10.1007/s12598-013-0134-x.

[41] J. Horcheni, K. Nouri, E. Dhahri, L. Bessais, Crystal structure, critical phenomena and magnetocaloric properties of Ni-substituted ferromagnetic Pr_2Fe_{17} intermetallic compound around room temperature, J. Solid State Chem. 326 (2023) 124219, https://doi.org/10.1016/j.jssc.2023.124219.